

Available online at [www.sciencedirect.com](http://www.sciencedirect.com)

ScienceDirect

[www.elsevier.com/locate/jmbbm](http://www.elsevier.com/locate/jmbbm)

## Research paper

# Mechanical characterization of brain tissue in simple shear at dynamic strain rates

Badar Rashid<sup>a</sup>, Michel Destrade<sup>b,a</sup>, Michael D. Gilchrist<sup>a,\*</sup><sup>a</sup>School of Mechanical and Materials Engineering, University College Dublin, Belfield, Dublin 4, Ireland<sup>b</sup>School of Mathematics, Statistics and Applied Mathematics, National University of Ireland Galway, Galway, Ireland

## ARTICLE INFO

## Article history:

Received 5 November 2012

Received in revised form

28 June 2013

Accepted 15 July 2013

Available online 24 July 2013

## Keywords:

Diffuse axonal injury (DAI)

Ogden

Mooney–Rivlin

Traumatic brain injury (TBI)

Homogeneous

Viscoelastic

Relaxation

## ABSTRACT

During severe impact conditions, brain tissue experiences a rapid and complex deformation, which can be seen as a mixture of compression, tension and shear. Diffuse axonal injury (DAI) occurs in animals and humans when both the strains and strain rates exceed 10% and 10/s, respectively. Knowing the mechanical properties of brain tissue in shear at these strains and strain rates is thus of particular importance, as they can be used in finite element simulations to predict the occurrence of brain injuries under different impact conditions. However, very few studies in the literature provide this information. In this research, an experimental setup was developed to perform simple shear tests on porcine brain tissue at strain rates  $\leq 120/s$ . The maximum measured shear stress at strain rates of 30, 60, 90 and 120/s was  $1.15 \pm 0.25$  kPa,  $1.34 \pm 0.19$  kPa,  $2.19 \pm 0.225$  kPa and  $2.52 \pm 0.27$  kPa, (mean  $\pm$  SD), respectively at the maximum amount of shear,  $K=1$ . Good agreement of experimental, theoretical (Ogden and Mooney–Rivlin models) and numerical shear stresses was achieved ( $p=0.7866$ – $0.9935$ ). Specimen thickness effects (2.0–10.0 mm thick specimens) were also analyzed numerically and we found that there is no significant difference ( $p=0.9954$ ) in the shear stress magnitudes, indicating a homogeneous deformation of the specimens during simple shear tests. Stress relaxation tests in simple shear were also conducted at different strain magnitudes (10–60% strain) with the average rise time of 14 ms. This allowed us to estimate elastic and viscoelastic parameters (initial shear modulus,  $\mu=4942.0$  Pa, and Prony parameters:  $g_1=0.520$ ,  $g_2=0.3057$ ,  $\tau_1=0.0264$  s, and  $\tau_2=0.011$  s) that can be used in FE software to analyze the non-linear viscoelastic behavior of brain tissue. This study provides new insight into the behavior in finite shear of brain tissue under dynamic impact conditions, which will assist in developing effective brain injury criteria and adopting efficient countermeasures against traumatic brain injury.

© 2013 Elsevier Ltd. All rights reserved.

## 1. Introduction

The human head is the most sensitive region involved in life-threatening injuries due to falls, traffic accidents and sports

accidents. Intracranial brain deformations are produced by rapid angular and linear accelerations as a result of blunt impact to the head, leading to traumatic brain injuries (TBIs) which remain a main cause of death and severe disabilities

\*Corresponding author. Tel.: +353 1 716 1884, +353 1 716 1991, +353 91 49 2344; fax: +353 1 283 0534.

E-mail addresses: [badar.rashid@ucdconnect.ie](mailto:badar.rashid@ucdconnect.ie) (B. Rashid), [michel.destrade@nuigalway.ie](mailto:michel.destrade@nuigalway.ie) (M. Destrade), [michael.gilchrist@ucd.ie](mailto:michael.gilchrist@ucd.ie) (M.D. Gilchrist).

around the world. During severe impact to the head, brain tissue experiences a mixture of compression, tension and shear which may occur in different directions and in different regions of the brain (Takhounts et al., 2003a; Nicolle et al., 2004, 2005). To gain a better understanding of the mechanisms of TBI, several research groups have developed numerical models which contain detailed geometric descriptions of the anatomical features of the human head. These models were used to investigate internal dynamic responses to multiple loading conditions (Claessens et al., 1997; Claessens, 1997; Ho and Kleiven, 2009; Horgan and Gilchrist, 2003; Kleiven, 2007; Kleiven and Hardy, 2002; Ruan et al., 1994; Takhounts et al., 2003b; Zhang et al., 2001). However, the biofidelity of these models is highly dependent on the accuracy of the material properties used to model biological tissues; therefore, a systematic investigation of the constitutive behavior of brain tissue under impact is essential.

The duration of a typical head impact is of the order of milliseconds. Therefore to model TBI, we need to characterize brain tissue properties over the expected range of loading rate appropriate for potentially injurious circumstances. Diffuse axonal injury (DAI) is characterized by microscopic damage to axons throughout the white matter of the brain, and by focal lesions in the corpus callosum and rostral brainstem and is considered as the most severe form of TBI (Anderson, 2000; Gennarelli et al., 1972; Margulies and Thibault, 1989; Ommaya et al., 1966). DAI in animals and humans has been estimated to occur at macroscopic shear strains of 10–50% and strain rates of approximately 10–50/s (Margulies et al., 1990; Meaney and Thibault, 1990). Several studies have been conducted to determine the range of strain and strain rates associated with DAI. Bain and Meaney (2000) investigated *in vivo*, tissue-level, mechanical thresholds for axonal injury and their predicted threshold strains for injury ranged from 0.13 to 0.34. Similarly, Pfister et al. (2003) developed a uniaxial stretching device to study axonal injury and neural cell death by applying strains within the range of 20–70% and strain rates within the range of 20–90/s to create mild to severe axonal injuries. Bayly et al. (2006) carried out *in vivo* rapid indentation of rat brain to determine strain fields using harmonic phase analysis and tagged MR images. Values of maximum principal strains  $>0.20$  and strain rates  $>40/s$  were observed in several animals exposed to 2 mm impacts of 21 ms duration. Studies conducted by Morrison et al. (2006, 2003, 2000) also suggested that the brain cells are significantly damaged at strains  $>0.10$  and strain rates  $>10/s$ .

Over the past 5 decades, several research groups investigated the mechanical properties of brain tissue in order to establish constitutive relationships over a wide range of loading conditions. Mostly dynamic oscillatory shear tests were conducted over a wide frequency range of 0.1–10,000 Hz (Arbogast et al., 1995, 1997; Arbogast and Margulies, 1998; Bilston et al., 1997; Brands et al., 1999, 2000a, 2000b, 2004; Darvish and Crandall, 2001; Fallenstein et al., 1969; Garo et al., 2007; Hirakawa et al., 1981; Hrapko et al., 2008; Nicolle et al., 2004, 2005; Prange and Margulies, 2002; Shen et al., 2006; Shuck and Advani, 1972; Thibault and Margulies, 1998) and various other techniques were used (Atay et al., 2008; LaPlaca et al., 2005; Lippert et al., 2004; Trexler et al., 2011) to determine the shear properties of the brain tissue. Similarly, unconfined

compression and tension tests were also performed by various research groups (Cheng and Bilston, 2007; Estes and McElhaney, 1970; Prange et al., 2000; Gefen and Margulies, 2004; Miller and Chinzei, 1997, 2002; Pervin and Chen, 2009; Prange and Margulies, 2002; Rashid et al., 2012b; Tamura et al., 2008, 2007; Velardi et al., 2006) to characterize the mechanical behavior of brain tissue at variable strain rates and the reported properties vary from study to study.

Bilston et al. (2001) performed *in vitro* constant strain rate oscillatory simple shear tests on bovine brain tissue (excised from corpus callosum region) using a parallel plate rotational rheometer and achieved strains up to 100% and strain rates of 0.055, 0.234, 0.95/s. Similarly, *in vitro* simple shear tests were performed on human and bovine brain tissues (gray and white matter regions) at a strain rate of 10/s and up to 50% strain by Takhounts et al. (2003a). Hrapko et al. (2006) also performed *in vitro* simple shear experiments on porcine brain tissue (white matter regions) using an oscillatory rotational rheometer with a strain amplitude of 0.01 and frequencies ranging from 0.04 to 16 Hz. The strain rates ranged from 0.01 to 1/s and strains up to 50%. In all these cases, the magnitudes of strain rates are below the axonal injury thresholds except at 10/s strain rate. Only the study conducted by Donnelly and Medige (1997) achieved engineering strain rates of 0, 30, 60 and 90/s with some additional tests performed at 120 and 180/s. They performed *in vitro* simple shear tests on cylindrical specimens of human brain tissue; however, these tests were completed within 2–5 days of postmortem. Therefore, the possibility of significant stiffness changes to the specimen cannot be ruled out due to this long postmortem time duration. Moreover, a two-term power equation ( $\sigma = Ae^B$ , where  $\sigma$  = shear stress,  $A$  = coefficient,  $B$  = exponent, and  $\epsilon$  = finite shear strain) was used to model the constitutive behavior of tissue. This can be improved to model simple shear. In particular, their power law constitutive equation is not physical for two reasons: (i) it is not an odd function of the shear strain, which would imply that shearing an isotropic material in one direction or its opposite requires forces with different magnitudes and (ii) it gives an initial slope of zero for the shear stress–strain curve, which would give a zero shear modulus or, equivalently in incompressible solids, a zero Young modulus.

In this study, the mechanical properties of porcine brain tissue have been determined by performing large simple shear tests at strain rates of 30, 60, 90 and 120/s. Due to the ready availability of porcine brains, all tests were completed within 8 h of postmortem. The experimental challenge with these tests was to attain uniform velocity during simple shearing of the brain tissue. To this end, a dedicated High Rate Shear Device (HRSD) was designed to achieve uniform velocity during dynamic tests (Rashid et al., 2012a). This study will provide new insight into the behavior of brain tissue under dynamic impact conditions, which would assist in developing effective brain injury criteria and adopting efficient countermeasures against TBI. Hyperelastic modeling of brain tissue was performed using Fung, Gent, Mooney–Rivlin and one-term Ogden models and the fundamental aspects of simple shear were considered based on recent studies (Destrade et al., 2008, 2012; Horgan, 1995; Horgan and Murphy, 2011; Horgan and Saccomandi, 2001; Merodio and Ogden, 2005). A non-linear viscoelastic analysis was also

carried out by performing stress relaxation tests. Finally, numerical simulations were performed in ABAQUS Explicit/6.9 using material parameters from the Mooney–Rivlin and one-term Ogden models in order to analyze the hyperelastic behavior of brain tissue.

## 2. Materials and methods

### 2.1. Experimental setup

A High Rate Shear Device (HRSD) was developed in order to perform large simple shear tests at dynamic strain rates of 30, 60, 90, and 120/s. As shown in Fig. 1(a) and (b), the major components of the apparatus include an electronic actuator (700 mm stroke, 1500 mm/s velocity, LEFB32T-700, SMC Pneumatics), one  $\pm 5$  N load cell (rated output: 1.46 mV/V nominal, GSO series, Transducer Techniques) and a Linear Variable Displacement Transducer (range  $\pm 25$  mm, ACT1000 LVDT, RDP Electronics). The load cell was calibrated against known masses and a multiplication factor of 13.67 N/V (determined through calibration) was used to convert voltage (V) to force (N). An integrated amplifier (AD 623 Gain,  $G=100$ , Analog Devices) with built-in single pole low-pass filters having cut-off frequencies of 10 kHz and 16 kHz was used. The amplified signal was analyzed through a data acquisition system (DAS) with a sampling frequency of 10 kHz.

The force (N) and displacement (mm) data against time (s) were recorded for the tissue experiencing the finite amount of shear,  $K=d/y$  ( $d$ =displacement of lower platen (mm) and  $y$ =thickness of specimen (mm)). The striker attached to the electronic actuator moved at a particular velocity to strike the shear pin which was rigidly attached to the lower platen through a rigid link as shown in Fig. 1(a). During the tests, the top platen remained stationary while the lower platen moved horizontally to produce the required simple shear in the specimen. The two output signals (displacement signal from LVDT and force signal from the load cell), as shown in Fig. 1(b), were captured simultaneously through the data acquisition system (DAS) at a sampling rate of 10 kHz. The pre-stressed LVDT probe was in continuous contact with the link to record the displacement during the shear phase of the tests. Two main contributing factors for the non-uniform

velocity were the deceleration of the electronic actuator when it approached the end of the stroke and the opposing forces acting against the striking mechanism. Therefore, the striking mechanism was designed and adjusted to ensure that it impacted the tension pin approximately 200 mm before the actuator came to a complete stop. The striker impact generated backward thrust, which was fully absorbed by the spring mounted on the actuator guide rod to prevent any damage to the programmable servo motor.

### 2.2. Specimen preparation and attachment

Ten fresh porcine brains from approximately 6 month old pigs were collected from a local slaughter house and tested within 8 h postmortem. Each brain was preserved in a physiological saline solution at 4–5 °C during transportation. All samples were prepared and tested at a nominal room temperature of 23 °C. The dura and arachnoid were removed and the cerebral hemispheres were first split into right and left halves by cutting through the corpus callosum and midbrain. As shown in Fig. 2, square specimens composed of mixed white and gray matter were prepared using a square steel cutter with sharp edges and nominal dimensions (20.0 mm: length  $\times$  20 mm: width). The extracted brain specimen was then inserted in a 4.0 mm thick square unit with inner dimension (19.0 mm: length  $\times$  19.0 mm: width) as shown in Fig. 2. The excessive brain portion was then removed with a surgical scalpel to maintain an approximate specimen thickness of  $4.0 \pm 0.1$  mm. All specimens were extracted from the cerebral halves while cutting from the medial to lateral direction. Two specimens were extracted from each cerebral hemisphere. The actual thickness of specimens measured before the testing was  $4.0 \pm 0.2$  mm (mean  $\pm$  SD). Forty specimens were prepared from 10 brains (four specimens from each brain). This allowed for a sample volume of 1.44 cm<sup>3</sup>, which was about half the average volume of the cylindrical samples tested by Donnelly and Medige (1997) and thus reduced heterogeneity effects.

The time elapsed between harvesting of the first and the last specimens from each brain was 17–20 min. Due to the softness and tackiness of brain tissue, each specimen was tested only once and no preconditioning was performed (Miller and Chinzei, 1997, 2002; Tamura et al., 2007; Velardi et al., 2006). Physiological

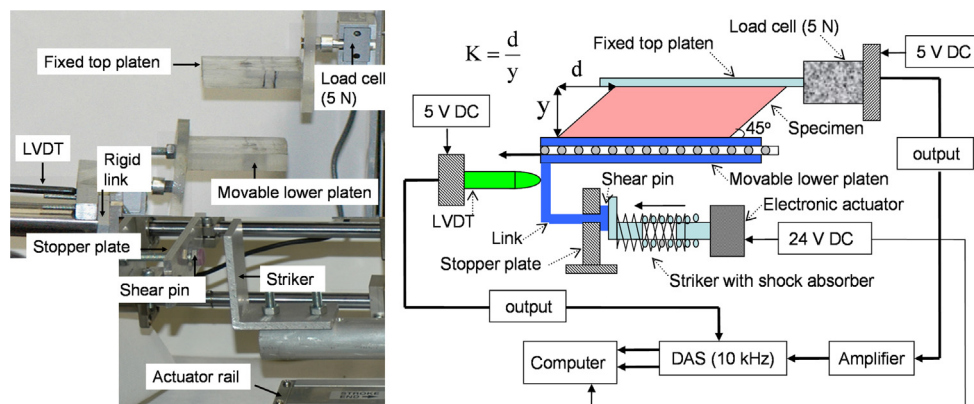
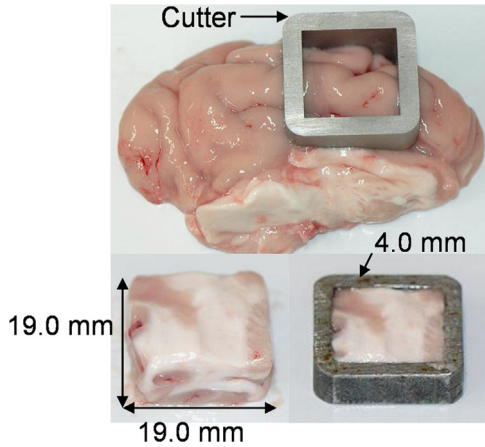
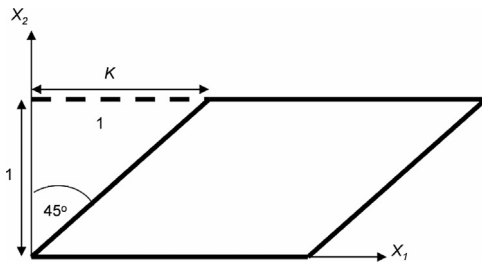


Fig. 1 – (a) Major components of high rate shear device (HRSD). (b) Schematic diagram of complete test setup.  $K=1$  for maximum amount of shear.



**Fig. 2** – Square specimen of brain tissue ( $19.0 \pm 0.1 \times 19.0 \pm 0.1$  mm) and  $4.0 \pm 0.1$  mm<sup>2</sup> thick excised from medial to lateral direction. A square steel cutter with the nominal dimensions (20.0 mm: length  $\times$  20.0 mm: width) was used for the excision. There was no abnormal deformation nor visible damage to the brain samples during the cutting process because the cutter was first dipped in a saline solution and then gradual force was applied to extract the specimens. The edges of the square cutter were very sharp which also facilitated smooth extraction of specimens. The prepared specimen is placed on a lower platen applied with a thin layer of surgical glue.



**Fig. 3** – Schematic of simple shear deformation at amount of shear  $K=1$ .

saline solution was applied to specimens frequently during cutting and before the tests in order to prevent dehydration. The specimens were not all excised simultaneously, rather each specimen was tested first and then another specimen was extracted from the cerebral hemisphere. This procedure was also important to prevent the tissue from losing some of its stiffness and to prevent dehydration, and thus contributed towards repeatability in the experimentation. Reliable attachment of brain tissue specimens was important in order to achieve high repeatability during simple shear tests. The surfaces of the platens were first covered with a masking tape substrate to which a thin layer of surgical glue (Cyanoacrylate, Low viscosity Z105880-1EA, Sigma-Aldrich) was applied. The prepared specimen of tissue was then placed on the lower platen. The top platen, which was attached to the 5 N load cell, was then lowered slowly so as to just touch the top surface of the specimen. One minute settling time was sufficient to ensure proper adhesion of the specimen to the platens. Finally, before

mounting brain specimens for simple shear tests, calibration of the HRSD was essential in order to ensure uniform velocity at each strain rate (30, 60, 90, and 120/s). During the calibration process, the actuator was run several times with and without any brain tissue specimen to ensure repeatability of displacement (mm) against time (s).

### 2.3. Stress relaxation tests in simple shear

A separate set of relaxation experiments was performed on square specimens ( $19.0 \times 19.0$  mm: width  $\times$  length) using a nominal thickness of 4.0 mm. Here, 40 specimens were extracted from 10 brains (four specimens from each brain). Stress relaxation tests were performed from 10% to 60% engineering strain in order to investigate the viscoelastic behavior of brain tissue. The specimens were shear tested from 30–174 mm/s to various strain levels and the data was acquired at a sampling rate of 10 kHz. The average rise time (ramp duration) measured from the stress relaxation experiments was 14 ms and the shear stress (Pa) vs. time (s) data was recorded up to 150 ms (hold duration). The relaxation data was required for the determination of time-dependent parameters such as  $\tau_k$ , the characteristic relaxation times, and  $g_k$ , the relaxation coefficients.

## 3. Constitutive models

### 3.1. Preliminaries

Let  $\underline{\mathbf{F}} = d\underline{\mathbf{x}}/d\underline{\mathbf{X}}$  be the deformation gradient tensor, where  $\underline{\mathbf{X}}$  is the position of a material element in the undeformed configuration and  $\underline{\mathbf{x}}$  is the corresponding position of the material element in the deformed configuration (Holzapfel, 2008; Ogden, 1997). In the Rectangular Cartesian coordinate system aligned with the edges of the specimen in its undeformed configuration, the simple shear deformation as shown in Fig. 3, can be written as

$$x_1 = X_1 + KX_2, \quad x_2 = X_2, \quad x_3 = X_3 \quad (1)$$

where  $K$  is the amount of shear. Using Eq. (1), the deformation gradient tensor  $\underline{\mathbf{F}}$  can be expressed as

$$\underline{\mathbf{F}} = \begin{bmatrix} 1 & K & 0 \\ 0 & 1 & 0 \\ 0 & 0 & 1 \end{bmatrix} \quad (2)$$

From Eq. (2), the right Cauchy–Green deformation tensor  $\underline{\mathbf{C}} = \underline{\mathbf{F}}^T \underline{\mathbf{F}}$  has thus the following components

$$\underline{\mathbf{C}} = \underline{\mathbf{F}}^T \underline{\mathbf{F}} = \begin{bmatrix} 1 & K & 0 \\ K & 1 + K^2 & 0 \\ 0 & 0 & 1 \end{bmatrix} \quad (3)$$

In general, an isotropic hyperelastic incompressible material is characterized by a strain-energy density function  $W$  which is a function of two principal strain invariants only:  $W = W(I_1, I_2)$ , where  $I_1$  and  $I_2$  are defined as (Ogden, 1997)

$$I_1 = \text{tr} \underline{\mathbf{C}}, \quad I_2 = \frac{1}{2}(I_1^2 - \text{tr}(\underline{\mathbf{C}}^2)) \quad (4)$$

But in the present case of simple shear deformation,

$$I_1 = I_2 = 3 + K^2 \quad (5)$$

The shear component of the Cauchy stress tensor is (Ogden, 1997)

$$\sigma_{12} = 2K \left( \frac{\partial W}{\partial I_1} + \frac{\partial W}{\partial I_2} \right) \quad (6)$$

so that

$$W = W(3 + K^2, 3 + K^2) = \hat{W}(K) \quad \text{say} \quad (7)$$

using the chain rule, we find

$$\hat{W}' = \frac{\partial(3 + K^2)}{\partial K} \frac{\partial W}{\partial I_1} + \frac{\partial(3 + K^2)}{\partial K} \frac{\partial W}{\partial I_2} = 2K \left( \frac{\partial W}{\partial I_1} + \frac{\partial W}{\partial I_2} \right) = \sigma_{12} \quad (8)$$

During simple shear tests, the amount of shear  $K$  was calculated from the measured displacement of the specimen in the transverse direction and the original thickness of the specimen. The tangential shear stress  $\sigma_{12}$  was evaluated as  $\sigma_{12} = F/A$ , where  $F$  is the shear force, measured in Newtons by the load cell, and  $A$  is the area of a cross-section of the specimen (length: 19.0 mm and width: 19.0 mm). Note that in simple shear, this area remains unchanged. The experimentally measured shear stress was then compared to the predictions of the hyperelastic models from the relation  $\sigma_{12} = \hat{W}'(K)$  (Ogden, 1997), and the material parameters were adjusted to give good curve fitting. Experimental shear stress values and the corresponding amount of shear  $K$  were used for the non-linear least-square fit of the parameters for four common hyperelastic constitutive models, presented in the next sections. The fitting procedure was performed using the `lsqcurvefit.m` function in MATLAB, and the quality of fit for each model was assessed based on the coefficient of determination,  $R^2$ . The fitting of hyperelastic models has been comprehensively covered by Ogden et al. (2004).

### 3.2. Fung strain energy function

The Fung isotropic strain energy (Fung, 1967; Fung et al., 1979) is often used for the modeling of isotropic soft biological tissues. It depends on the first strain invariant only as given below:

$$W = \frac{\mu}{2b} [e^{b(I_1-3)} - 1] \quad (9)$$

It yields the following simple shear stress component  $\sigma_{12}$  along the  $x_1$ -axis:

$$\sigma_{12} = \hat{W}'(K) = \mu K e^{bK^2} \quad (10)$$

Here  $\mu > 0$  (infinitesimal shear modulus) and  $b > 0$  (stiffening parameter) are the two constant material parameters to be adjusted in the curve-fitting exercise.

### 3.3. Gent strain energy function

The Gent isotropic strain energy (Gent, 1996) is often used to describe rapidly strain-stiffening materials. It also depends on the first strain invariant only, in the following manner:

$$W(I_1) = -\frac{\mu}{2} J_m \ln \left( 1 - \frac{I_1 - 3}{J_m} \right) \quad (11)$$

It yields the following shear component of the Cauchy stress:

$$\sigma_{12} = \hat{W}'(K) = \frac{\mu J_m K}{J_m - K^2} \quad (12)$$

Here  $\mu > 0$  (infinitesimal shear modulus) and  $J_m > 0$  are two constant material parameters to be optimized in the fitting exercise.

### 3.4. Mooney–Rivlin strain energy function

Mooney and Rivlin (Holzapfel, 2008; Mooney, 1964; Ogden, 1997) observed that the shear stress response of rubber was linear under large simple shear loading conditions. The same concept can be applied to brain tissue also to evaluate the accuracy and predictive capability of this model. Its strain energy density depends on the first and second strain invariants as given below:

$$W(I_1) = C_1(I_1 - 3) + C_2(I_2 - 3) \quad (13)$$

It yields the following shear component of the Cauchy stress tensor:

$$\sigma_{12} = \hat{W}'(K) = 2(C_1 + C_2)K \quad (14)$$

Here  $C_1 > 0$  and  $C_2 \geq 0$  are two material constants. They are related to the infinitesimal shear modulus as  $\mu = 2(C_1 + C_2)$ .

### 3.5. Ogden strain energy function

The Ogden model (Ogden, 1972) has been used previously to describe the non-linear mechanical behavior of brain matter, as well as of other non-linear soft tissues (Brittany and Margulies, 2006; Lin et al., 2008; Miller and Chinzei, 2002; Prange and Margulies, 2002; Velardi et al., 2006). Soft biological tissue is often modeled well by the Ogden formulation and most of the mechanical test data available for brain tissue in the literature are, in fact, fitted with an Ogden hyperelastic function. The one-term Ogden hyperelastic function is given by

$$W = \frac{2\mu}{\alpha^2} (\lambda_1^\alpha + \lambda_2^\alpha + \lambda_3^\alpha - 3) \quad (15)$$

where the  $\lambda_i$  are the principal stretch ratios (the square roots of the eigenvalues of  $\mathbf{C}$ ).

In simple shear

$$\lambda_1 = \frac{K}{2} + \sqrt{1 + \frac{K^2}{4}}, \lambda_2 = \lambda_1^{-1} = -\frac{K}{2} + \sqrt{1 + \frac{K^2}{4}}, \lambda_3 = 1 \quad (16)$$

so that

$$\hat{W}(K) = \frac{2\mu}{\alpha^2} \left[ \left( \frac{K}{2} + \sqrt{1 + \frac{K^2}{4}} \right)^\alpha + \left( -\frac{K}{2} + \sqrt{1 + \frac{K^2}{4}} \right)^\alpha - 2 \right] \quad (17)$$

and the Cauchy shear stress component  $\sigma_{12}$  is

$$\sigma_{12} = \hat{W}'(K) = \frac{\mu}{\alpha} \frac{1}{\sqrt{1 + (K^2/4)}} \left[ \left( \frac{K}{2} + \sqrt{1 + \frac{K^2}{4}} \right)^\alpha - \left( -\frac{K}{2} + \sqrt{1 + \frac{K^2}{4}} \right)^\alpha \right] \quad (18)$$

When  $\alpha = 2$ , it reduces to  $\sigma_{12} = \mu K$  (linear) and recovers the Mooney–Rivlin material with  $C_2 = 0$ . Here,  $\mu > 0$  is the infinitesimal shear modulus, and  $\alpha$  is a stiffening parameter.

### 3.6. Viscoelastic modeling

Biological tissues usually exhibit non-linear behavior beyond 2–3% strain. Many non-linear viscoelastic models have been formulated, but Fung's theory (Fung, 1993) of quasi-linear

viscoelasticity (QLV) is probably the most widely used due to its simplicity. To account for the time-dependent mechanical properties of brain tissue, the stress–strain relationship is expressed as a single hereditary integral and a similar approach has been adopted earlier (Elkin et al., 2011; Finan et al., 2012; Miller and Chinzei, 2002). For a Mooney–Rivlin viscoelastic model, we have

$$S(t) = \mu \int_0^t G(t-\tau) \left( \frac{dK}{d\tau} \right) d\tau \quad (19)$$

Here,  $S(t)$  is the nominal shear stress component and  $\mu = 2(C_1 + C_2)$  is the initial shear modulus in the undeformed state, derived from the Mooney–Rivlin model (Eqs. (13) and (14)), where  $C_1 + C_2 > 0$ . Note that because the cross-sectional area remains unchanged in simple shear (Ogden, 1997), we have  $S(t) = \sigma_{12}(t)$ , the Cauchy shear stress component. The relaxation function  $G(t)$  is defined in terms of Prony series parameters

$$G(t) = \left[ 1 - \sum_{k=1}^n g_k (1 - e^{-t/\tau_k}) \right] \quad (20)$$

where  $\tau_k$  are the characteristic relaxation times, and  $g_k$  are the relaxation coefficients. In order to estimate material parameters with a physical meaning, we propose to solve Eq. (19) in two simple steps as discussed in Section 4.3. Similarly, the Ogden-based viscoelastic model can be expressed as follows:

$$S(t) = \frac{\mu}{\alpha} \int_0^t G(t-\tau) \frac{d}{d\tau} \left( \frac{1}{\sqrt{1 + (K^2/4)}} \left[ \left( \frac{K}{2} + \sqrt{1 + \frac{K^2}{4}} \right)^\alpha - \left( -\frac{K}{2} + \sqrt{1 + \frac{K^2}{4}} \right)^\alpha \right] \right) d\tau \quad (21)$$

## 4. Results

### 4.1. Experimentation

All simple shear tests were performed on brain specimens containing mixed white and gray matter. The shear tests were performed up to a maximum amount of shear,  $K=1$ , i.e., to an angle of  $45^\circ$ . This level of shear corresponds to an extension of 62% according to Eq. (16). The velocity of the electronic actuator was adjusted to displace the lower platen at the required velocity of 120, 240, 360 and 480 mm/s corresponding to approximate engineering strain rates of

30, 60, 90 and 120/s, respectively. The shear force (N) was sensed by the load cell attached to the top platen as discussed in Section 2.1 and the force–time data obtained at each strain rate was recorded at a sampling rate of 10 kHz. The force (N) was divided by the surface area in the reference configuration to determine shear stress in the tangential direction (along the  $x_1$ -axis, as shown in Fig. 4). Note that because this surface is normal to the plane of shear, its area remains unchanged and the shear components of the Cauchy and nominal stresses coincide. Each specimen was tested once and then discarded because of the highly dissipative nature of brain tissue.

Ten tests were performed at each strain rate as shown in Fig. 5, in order to investigate experimental repeatability and the behavior of tissue at a particular loading velocity. The shear force (N) vs. time curves increased monotonically at all strain rates.

During simple shear tests, the achieved strain rates were  $30 \pm 0.55/s$ ,  $60 \pm 1.89/s$ ,  $90 \pm 1.78/s$  and  $120 \pm 3.1/s$  (mean  $\pm$  SD) against the required loading velocities of 120, 240, 360 and 480 mm/s, respectively. It was observed that the tissue stiffness increased slightly with the increase in loading velocity, indicating stress–strain rate dependency of brain tissue. Moreover, shear stress profiles are significantly linear at 30, 60 and 120/s strain rates, but this behavior is not quite observed in the case of the 90/s strain rate. The maximum shear stress at strain rates of 30, 60, 90 and 120/s was  $1.15 \pm 0.25$  kPa,  $1.34 \pm 0.19$  kPa,  $2.19 \pm 0.225$  kPa and  $2.52 \pm 0.27$  kPa (mean  $\pm$  SD), respectively as shown in Fig. 5.

### 4.2. Fitting of constitutive models

The average shear stress (Pa) – amount of shear,  $K$  (engineering shear strain) curves at each loading rate as shown in Fig. 5, were fitted to the hyperelastic isotropic constitutive models (Fung, Gent, Mooney–Rivlin and Ogden models) presented in Section 3. Fitting of each constitutive model to experimental data is shown in Fig. 6. Good fitting is achieved for the Fung and Ogden models (coefficient of determination:  $0.9883 < R^2 \leq 0.9997$ ); however, the Mooney–Rivlin and Gent models could not provide as good a fitting ( $R^2 < 0.9899$ ) to shear data, particularly at a strain rate of 90/s due to the non-linear behavior of the shear stress–amount of the shear curve. Material parameters of the four constitutive models ( $\mu, \alpha, b, J_m, C_1, C_2$ ) were derived after fitting to average and

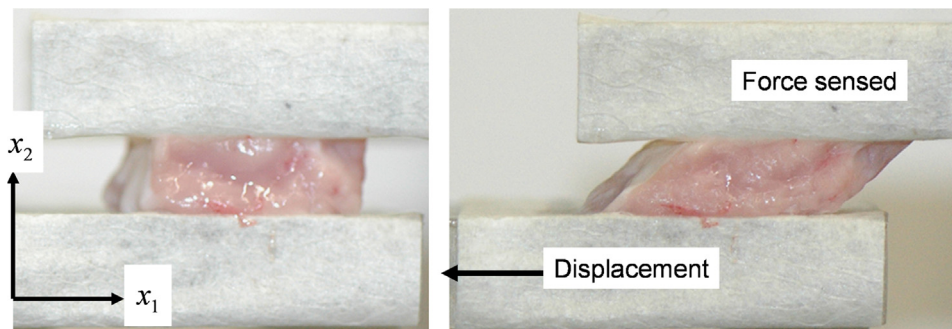
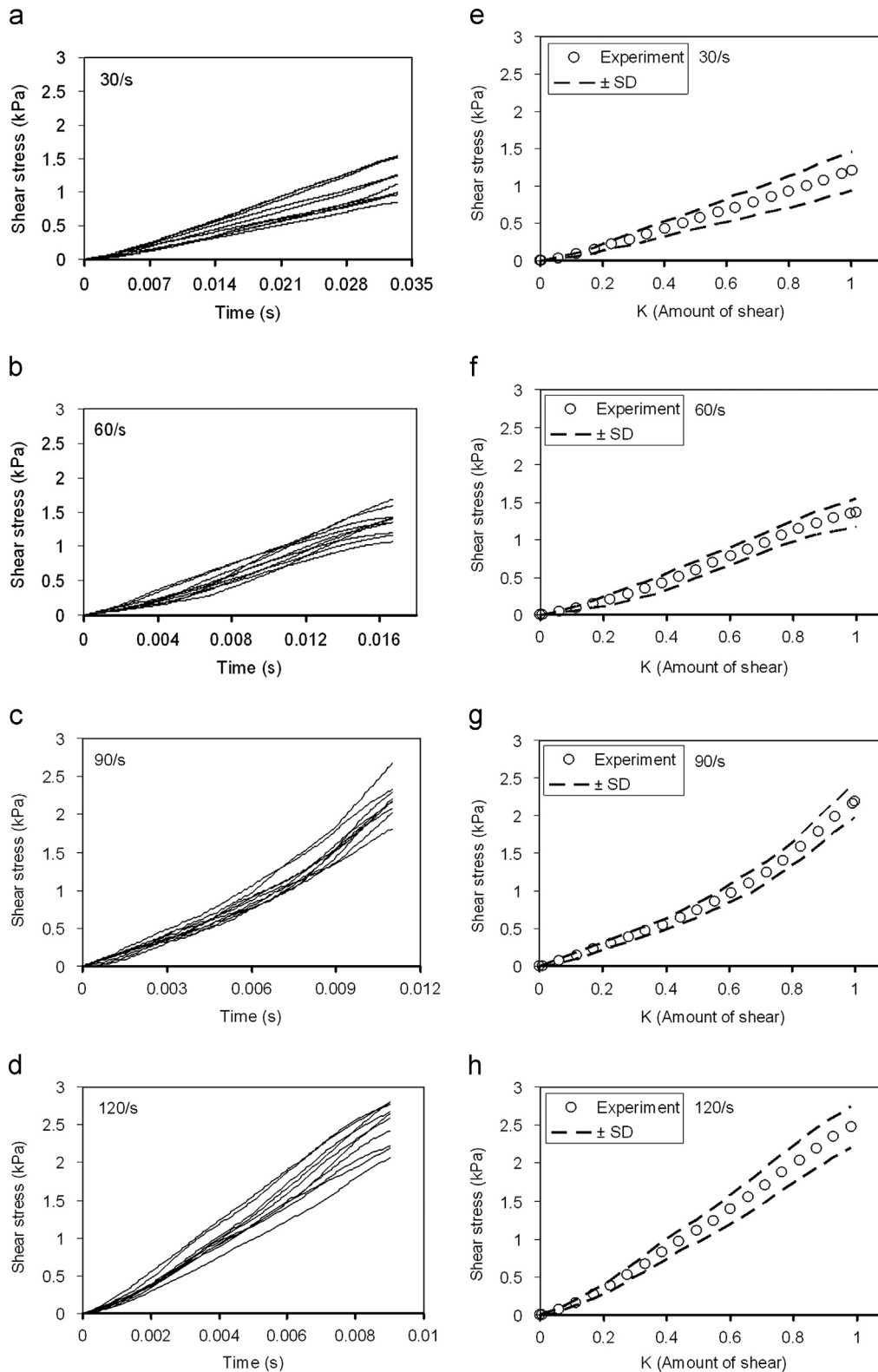


Fig. 4 – The brain specimen is attached between platens using a thin layer of surgical glue. Tissue deformations before and after completion of a simple shear test are shown.



**Fig. 5 – Experimental shear stress profiles at each strain rate (left) and corresponding average stresses and standard deviations (SD) (right).**

standard deviation ( $\pm$ SD) shear stress curves and these are summarized in [Table 1](#). The Mooney–Rivlin is a linear shear response model ( $\sigma_{12} = 2(C_1 + C_2)K$ ) and is best suited to fit linear experimental shear data as observed at strain rates of

30, 60 and 120/s; however, the Ogden model is suitable for both linear and non-linear experimental shear data as shown in [Fig. 6](#). If we consider for instance the Ogden model, we see that the initial shear modulus  $\mu$  increases by 9.3%, 11.6% and

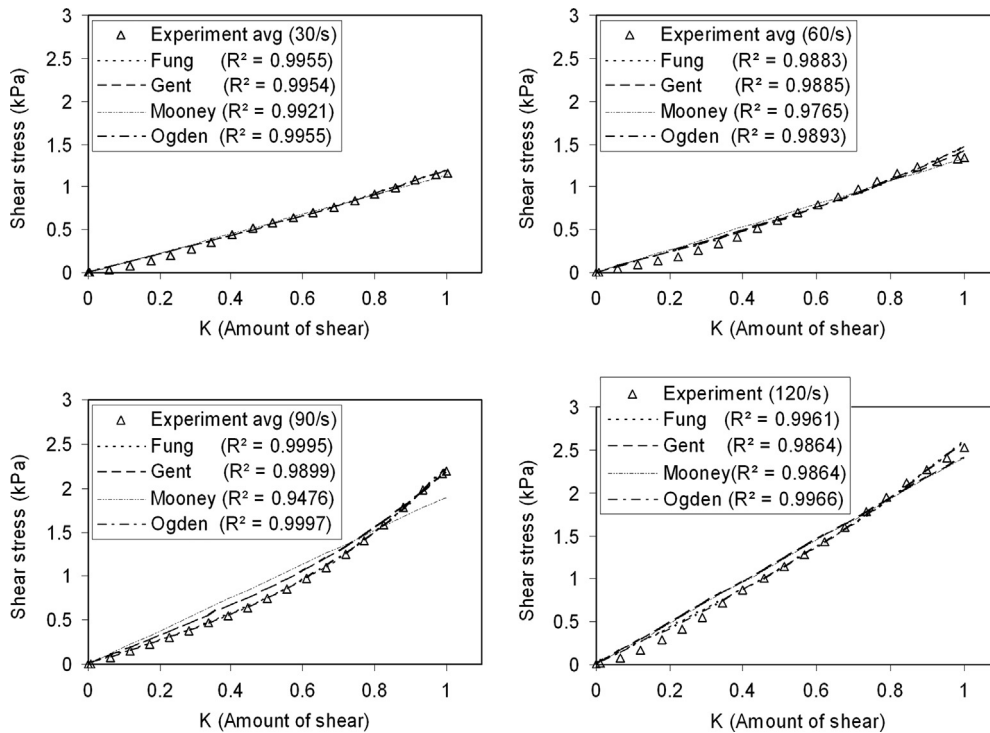


Fig. 6 – Fitting of strain energy functions to average experimental shear data at variable strain rates.

63.6% with the increase in strain rates from 30 to 60/s, 60 to 90/s and 90 to 120/s, respectively (Table 1). A similar increase in  $\mu$  is also observed in the case of the Fung, Gent and Mooney–Rivlin models. The significant increase in  $\mu$  with increasing strain rate clearly indicates that a viscoelastic model is required here. Note that the curve fitting exercise for the Mooney–Rivlin model only gives access to  $(C_1 + C_2)$ , and not to  $C_1$  and  $C_2$  independently.

#### 4.3. Estimation of viscoelastic parameters

During the stress relaxation tests, the displacement against time was directly recorded through a linear variable displacement transducer (LVDT) and the force (N) was measured directly through the load cell. The relaxation tests were performed at a high loading velocity in order to achieve a minimum rise time,  $t$ , approximately 14 ms, as shown in Fig. 7(a) and (b). However, it was not practically possible to achieve an ideal step response (time,  $t=0$ ). Therefore, back-extrapolation using *interp1* was performed in order to eliminate any error introduced by the ramp relaxation tests (Funk et al., 2000). Laksari et al. (2012) followed a similar approach and determined the instantaneous elastic stress response for the ideal step using a direct numerical integration scheme. However, in this study, extrapolated data was used to generate isochrones (shear stress values at different strain magnitudes but at the same time,  $t=0$ ) as shown in Fig. 7(c). Curve fitting of the Mooney–Rivlin model (Eq. (14)) was performed using average isochrones to derive  $C_1+C_2$ , thus directly giving the initial shear modulus  $\mu = 2(C_1+C_2)$  which is independent of time as shown in Fig. 7(d). Thereafter, Eq. (19) was convenient to implement in Matlab (Mathworks) by using the *gradient* and *conv* functions. The *gradient* function was used in order to determine the velocity

vector ( $dK/d\tau$ ) from the experimentally measured displacement,  $K$  and time,  $\tau$ . Also a *conv* function was used to convolve the relaxation function

(Eq. (20)) with the velocity vector, ( $dK/d\tau$ ). The coefficients of the relaxation function were optimized using *nlinfit* and *lsqcurvefit* to minimize error between the experimental stress data and Eq. (20). The sum of the Mooney–Rivlin constants is  $C_1+C_2=2471.1$  Pa and the corresponding shear modulus is thus  $\mu=4942.0$  Pa. Similarly, we estimated the Prony parameters ( $g_1=0.520$ ,  $g_2=0.3057$ ,  $\tau_1=0.0264$  s, and  $\tau_2=0.011$  s) from the two-term relaxation function (coefficient of determination:  $0.9891 < R^2 \leq 0.9934$ ) using the Matlab functions discussed above. These material parameters can then be used directly in FE software such as ABAQUS in order to analyze the non-linear viscoelastic behavior of brain tissue. As can be observed by inspection of Eq. (21), the corresponding procedure for the one-term Ogden material is much more involved, and it has not been conducted here.

## 5. Finite element analysis

### 5.1. Numerical and experimental results

A brain tissue specimen geometry (length  $\times$  width  $\times$  thickness = 19.0 mm  $\times$  19.0 mm  $\times$  4.0 mm) was developed using the finite element software ABAQUS 6.9 Explicit for numerical simulations. 2166  $\times$  C3D8R elements (Continuum, three-dimensional, eight-node linear brick, reduced integration) with default hourglass control were used for the brain part. The mass density 1040 kg/m<sup>3</sup> and material parameters listed in Table 1 for the Mooney–Rivlin and Ogden strain energy functions

**Table 1 – Material parameters derived after fitting of models,  $\mu$  (Pa), (mean with 95% confidence bound).**

Strain rate (1/s)	Fung model			Gent model		
	$\mu$	$b$	$R^2$	$\mu$	$J_m$	$R^2$
30	1047±258	0.122±0.022	0.9955	1050±257	9.0±1.8	0.9954
60	1157±210	0.229±0.04	0.9883	1197±228	6.7±2.2	0.9885
90	1322±156	0.520±0.03	0.9995	1594±393	3.7±1.23	0.9899
120	2104±347	0.211±0.067	0.9961	2414±630	5.6±1.3	0.9864
	Mooney–Rivlin model			Ogden model		
	$C_1 + C_2$		$R^2$	$\mu$	$\alpha$	$R^2$
30	567.5±207		0.9921	1038±258	2.766±0.21	0.9957
60	665.5±214		0.9765	1135±215	3.338±0.24	0.9893
90	947.7±188		0.9476	1267±182	4.576±0.18	0.9997
120	1166.6±160		0.9864	2073±351	3.231±0.32	0.9966

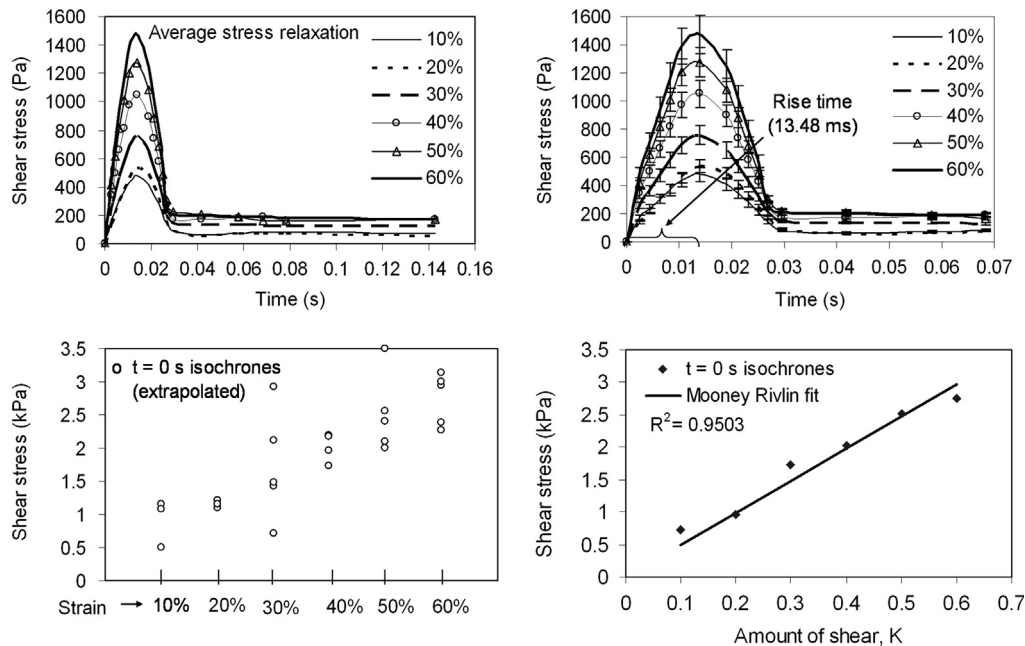


**Fig. 7 – Stress relaxation experiments in simple shear at different strain magnitudes, with average rise time of 13.48 ms. (a) Relaxation data up to 140 ms during hold period, (b) average rise time (13.48 ms) at different strains, (c) isochronous data after extrapolation, and (d) fitting of Mooney–Rivlin model to average isochrones.**

were used for numerical simulations. The top surface of the specimen was constrained in all directions whereas the lower surface was allowed to be displaced only in the lateral direction ( $x_1$ -axis) in order to achieve the maximum amount of shear,  $K=1$  for all simulations. Mesh convergence analysis was also carried out by varying mesh density before validating the results. The mesh was considered convergent when there was a negligible change in the numerical solution (0.6%) with further mesh refinement and the average simulation time was approximately 50 s.

Simulations were performed in order to determine the force (N) on the top surface of the specimen (along the  $x_1$ -axis or the tangential direction) and were compared with the experimental force (N) measured directly during simple shear tests. A similar procedure was also adopted to compare shear

stresses (kPa) as shown in Fig. 8. Based on the statistical analysis using a one-way ANOVA test, a good agreement was achieved between the experimental and numerical results (Ogden and Mooney–Rivlin models) as shown in Table 2.

### 5.2. Homogeneity of the fields

Shear stress contours provided by the numerical simulations were also examined. The comparison was carried out for the material parameters at different strain rates using the one-term Ogden model as shown in Fig. 9. The shear stress concentration is conspicuous at the two opposite corners (or edges) on the diagonal with maximum stretched length as depicted in Fig. 9(a). However, these effects are

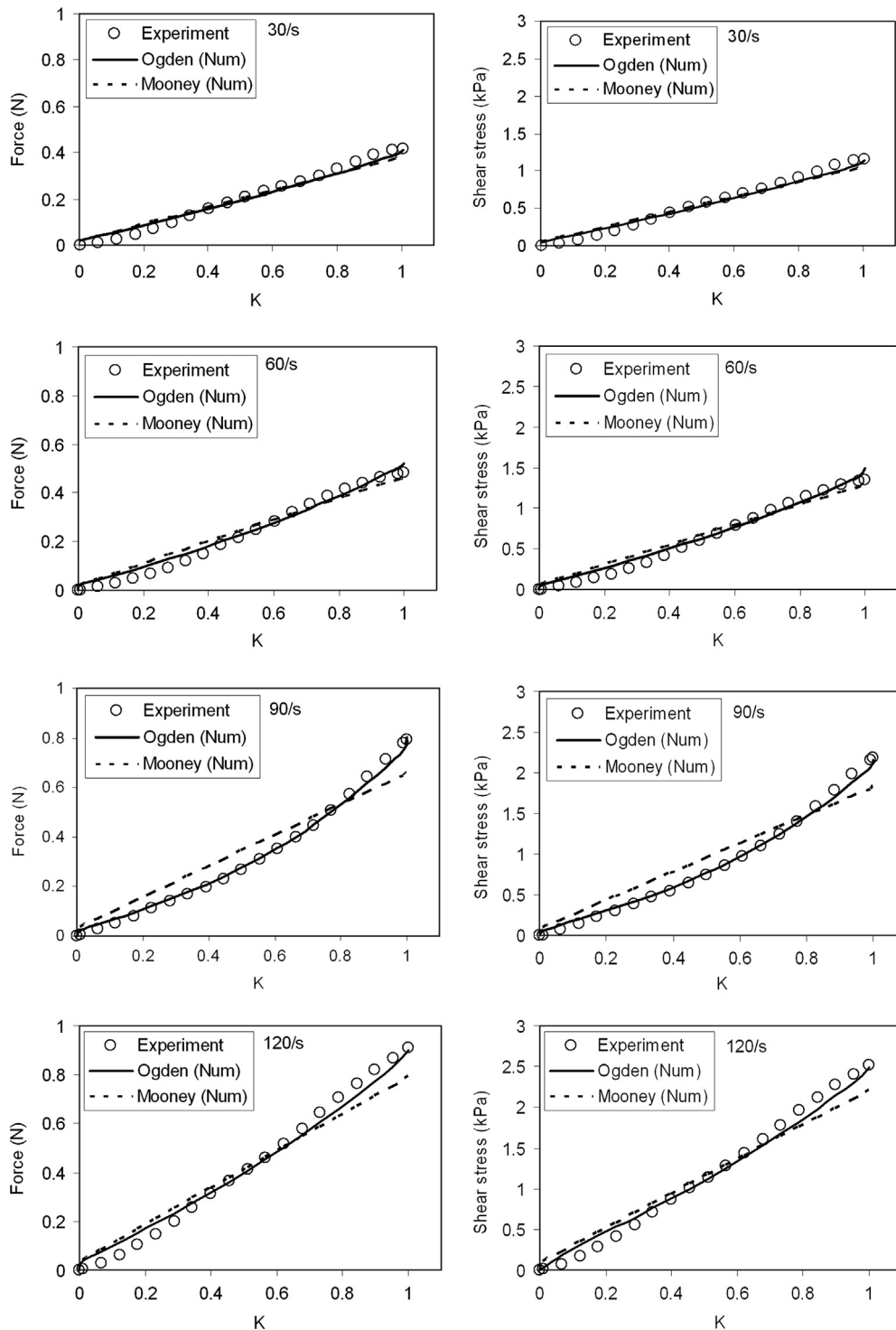


Fig. 8 – Comparison of shear forces (N) and shear stresses (kPa) at different strain rates.

localized and of small amplitude, so that a globally homogeneous stress behavior is observed over the larger volume of the specimen in all the cases. A similar procedure was adopted to compare force (N) contours at each strain rate. The negative force magnitudes are observed on each node at the lower sliding surface of the specimen whereas positive reaction forces are noticed on the top surface of the specimen, which was expected under simple shear deformations (so called Poynting effect, see [Ogden](#)

(1997)). The homogeneous force pattern is achieved at each strain rate.

### 5.3. Specimen thickness effects in simple shear

Numerical simulations were also performed at variable specimen thicknesses (2.0, 3.0, 4.0, 7.0 and 10.0 mm) in order to analyze thickness effects. Simulations were performed using the one-term Ogden parameters obtained from the

**Table 2 – Statistical comparison of experimental and numerical forces (N) and stresses (kPa) using one-way ANOVA test based on Fig. 7.**

Strain rate (1/s)	Experimental force (N)		Experimental stress (kPa)	
	Ogden (numerical)	Mooney (numerical)	Ogden (numerical)	Mooney (numerical)
30/s	$p=0.9793$	$p=0.9864$	$p=0.9791$	$p=0.9803$
60/s	$p=0.8268$	$p=0.8169$	$p=0.8201$	$p=0.7974$
90/s	$p=0.9752$	$p=0.7928$	$p=0.9935$	$p=0.7866$
120/s	$p=0.9950$	$p=0.9338$	$p=0.9830$	$p=0.9553$

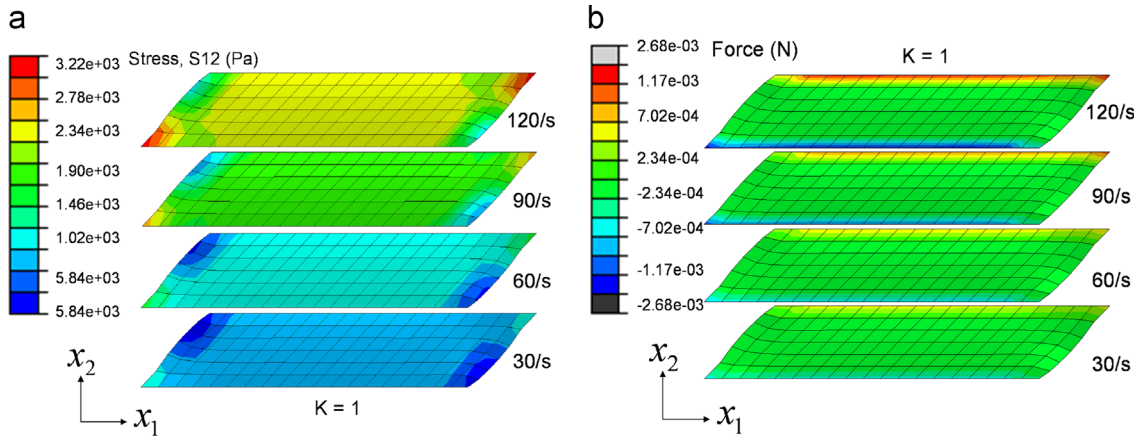


**Fig. 9 – Simple shear deformation using the Ogden parameters (a) contours of shear stress (Pa) and (b) contours of force (N).**

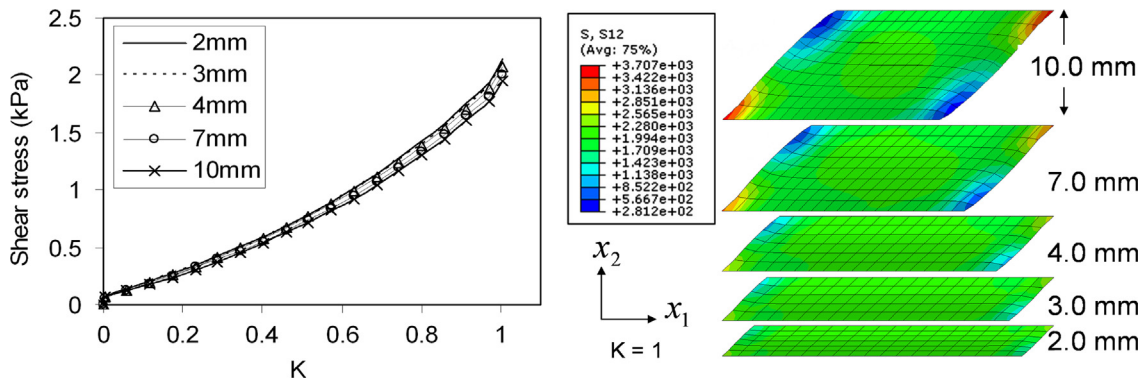


**Fig. 10 – Consistency in shear stress profiles at variable sample thickness using the Ogden material parameters obtained at a strain rate of 90/s.**

experimental data at a strain rate of 90/s as shown in Fig. 10; however similar behavior can also be observed at other strain rates. Based on a statistical analysis, using a one-way ANOVA test, it is interesting to note that there is no significant difference ( $p=0.9954$ ) in the shear stress magnitudes between specimens of different thicknesses (2.0–10.0 mm). The consistency in shear stress magnitudes, as indicated in Fig. 10, clearly indicates globally homogeneous deformation of the specimen and the results are independent of specimen thickness.

Therefore, the results of the simple shear test protocol can be considered to be much more reliable than those of the compression and tension test protocols adopted by various research groups (Cheng and Bilston, 2007; Estes and

McElhane, 1970; Miller and Chinzei, 1997, 2002; Pervin and Chen, 2009; Prange and Margulies, 2002; Rashid et al., 2012b; Tamura et al., 2008, 2007; Velardi et al., 2006). Compression and tension tests of brain matter display a strong sensitivity to non-homogeneity and sample thickness, and do not allow for strains as large as those achieved in simple shear (according to Eq. (16), when  $K=1$ ,  $\lambda_1 = (1 + \sqrt{5})/2 = 1.62$ , i.e. an extension of 62%).

## 6. Discussion

Simple shear tests were successfully performed on porcine brain tissue at variable strain rates (30, 60, 90 and 120/s) on a

custom designed HRSD, within 8 h postmortem. These strain rates entirely cover the range associated with DAI (Bain and Meaney, 2000; Bayly et al., 2006; Margulies et al., 1990; Meaney and Thibault, 1990; Morrison et al., 2006; 2003, 2000; Pfister et al., 2003). However, in order to obtain viscoelastic material parameters for the brain tissue, stress relaxation tests were also performed at various strain magnitudes as discussed in Section 4.3. The proposed elastic and viscoelastic parameters ( $\mu=4942.0$  Pa and Prony parameters:  $g_1=0.520$ ,  $g_2=0.3057$ ,  $\tau_1=0.0264$  s, and  $\tau_2=0.011$  s) can be used directly in FE software to analyze the non-linear viscoelastic behavior of brain tissue modeled as a Mooney–Rivlin material.

Special attention was paid to maintain uniform velocity and a constant strain during the stress relaxation tests at each loading rate by calibrating the HRSD before the tests. Fig. 11 shows the start and end of a typical simple shear test indicated between points A and B, respectively. The DAS as discussed in Section 2.1 was able to capture force and displacement signals directly.

During the calibration process, the measured displacement signal was checked precisely against the actual displacement of the shear pin. At this preparatory stage, the velocity of the actuator was adjusted with precision to attain a required strain rate. A linear displacement–time profile between points A and B (~4.0 mm displacement) precludes the possibility of any stoppages or irregular movements due to frictional effects between the reciprocating components (see Fig. 11). The movement of the LVDT stops at point B, however the DAS continuously measures the displacement and force signals. The displacement signal measured at point B and onward indicates no relative displacements between the top and bottom platens (acquiring constant strain) during simple shear tests. The brain tissue in simple shear under constant strain conditions starts relaxing with the increase in time (stress relaxation) as shown in Fig. 11. Separate relaxation tests were also performed at different strain magnitudes (10–60%).

It is noticed that the response in simple shear is almost linear for most of the strain rates, which somewhat contradicts previous work by e.g. Franceschini et al. (2006). The constants of the Ogden model used by Franceschini et al. lead to a material that is shear-stiffening, whereas the Mooney–Rivlin gives a linear stress–strain curve. However, their modeling was based on uniaxial compression/tension of human brain samples with glued ends, for which homogeneous

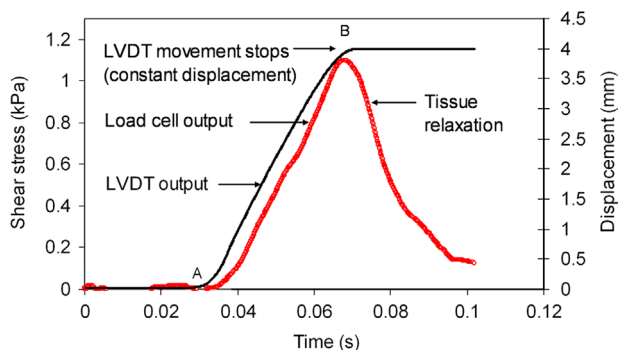


Fig. 11 – Typical output from data acquisition system (DAS) indicating force (N) and displacement (mm) signals.

deformations are not possible. In our work, on the other hand, we have achieved homogeneity in a very satisfying way by performing simple shear tests on porcine brain tissue.

Good agreement was achieved between the theoretical, numerical and experimental results, particularly in the case of the Ogden model, which is deemed suitable for both the linear and non-linear experimental shear data. However, the Mooney–Rivlin model was good for the linear experimental shear data only. Homogeneous deformation was achieved during simple shear tests and the magnitude of shear stress was proved to be independent of specimen thickness. The maximum shear stress (at  $K=1$ ) obtained at strain rates of 30, 60, 90 and 120/s was  $1.15 \pm 0.25$  kPa,  $1.34 \pm 0.19$  kPa,  $2.19 \pm 0.225$  kPa,  $2.52 \pm 0.27$  kPa, (mean  $\pm$  SD), respectively. Donnelly and Medige (1997) also performed *in vitro* simple shear tests on human brain tissue at the same strain rate range (30–90/s), but the magnitudes of their stresses were 3–4 times higher as compared to this study, as shown in Fig. 12. However, a direct comparison of their results with those obtained here cannot be performed because of a mistake they made in measuring the shear stresses (they multiplied  $\sigma_{12}$  by  $\sqrt{1+K^2}$  to account for “a reduced area of the sample due to stretching” when in fact this area remains unchanged in simple shear).

Based on numerical simulations, it is observed that the shear stresses are independent of specimen thickness, which shows homogeneous deformation of the brain tissue specimen up to  $K=1$ . Therefore, derived material parameters using a simple shear test protocol are more reliable than compression and tension test protocols adopted earlier (Cheng and Bilston, 2007; Estes and McElhaney, 1970; Miller and Chinzei, 1997, 2002; Pervin and Chen, 2009; Prange and Margulies, 2002; Rashid et al., 2012b; Tamura et al., 2008, 2007; Velardi et al., 2006).

A limitation of this study is that the estimation of material parameters from the strain energy functions is based on average mechanical properties (mixed white and gray matter) of the brain tissue; however, these results are still useful in modeling the approximate behavior of brain tissue. For instance, the average mechanical properties were also determined by Miller and Chinzei (1997, 2002). In previous studies, it was observed that the anatomical origin or location as well as the direction of excision of samples (superior–inferior and medial–lateral direction) had no significant effect on the

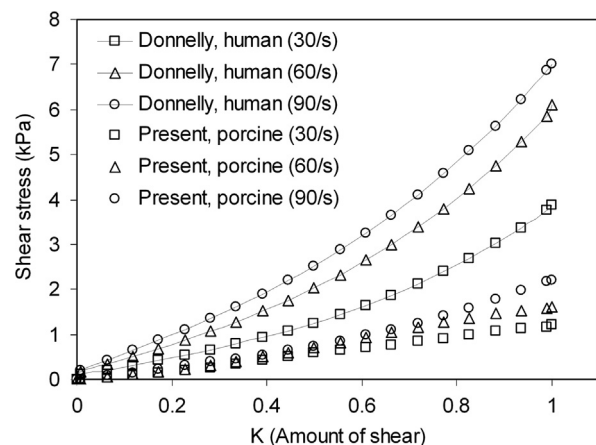


Fig. 12 – Comparison of simple shear stress (kPa) profiles with data of Donnelly and Medige (1997).

results (Tamura et al., 2007) and similar observations were also reported by Donnelly and Medige (1997) who used specimens with an average volume almost twice the average volume of the specimens used here. Therefore inter-regional variations were not investigated in the present research; however inter-specimen variations are clearly evident from the experimental data at each strain rate as shown in Fig. 5.

## 7. Conclusions

The following results can be concluded from this study:

- 1 Good agreement was achieved between the theoretical, numerical and experimental results, particularly in the case of the Ogden model ( $p=0.8201-0.9830$ ) which was suitable for representing both linear and non-linear experimental shear data. However, the Mooney–Rivlin model was good for the linear experimental shear data only ( $p=0.7866-0.9803$ ).
- 2 An approach adopted for the estimation of viscoelastic parameters can be adopted for the Ogden model also. The derived elastic and viscoelastic parameters ( $\mu=4942.0$  Pa and Prony parameters:  $g_1=0.520$ ,  $g_2=0.3057$ ,  $\tau_1=0.0264$  s, and  $\tau_2=0.011$  s) can be used directly in FE software to analyze the non-linear viscoelastic behavior of brain tissue.
- 3 The high rate shear experimental setup developed for simple shear tests of porcine brain tissue can be used with confidence at dynamic strain rates (30–120/s).

## Acknowledgments

The authors thank Dr. John D. Finan of Columbia University for his valuable input regarding implementation of the non-linear viscoelastic model. This work was supported for the first author by a Postgraduate Research Scholarship awarded in 2009 by the Irish Research Council for Science, Engineering and Technology (IRCSET), Ireland, and for the second author, by a New Foundations award from the Irish Research Council (IRC).

## REFERENCES

- Anderson, R., 2000. A Study of the Biomechanics of Axonal Injury. Ph.D. dissertation. University of Adelaide, South Australia.
- Arbogast, K., Meaney, D., Thibault, L., 1995. Biomechanical Characterization of the Constitutive Relationship for the Brainstem. SAE Technical Paper 952716.
- Arbogast, K.B., Margulies, S.S., 1998. Material characterization of the brainstem from oscillatory shear tests. *Journal of Biomechanics* 31, 801–807.
- Arbogast, K.B., Thibault, K.L., Pinheiro, B.S., Winey, K.I., Margulies, S.S., 1997. A high-frequency shear device for testing soft biological tissues. *Journal of Biomechanics* 30, 757–759.
- Atay, S.M., Kroenke, C.D., Sabet, A., Bayly, P.V., 2008. Measurement of the dynamic shear modulus of mouse brain tissue in vivo by magnetic resonance elastography. *Journal of Biomechanical Engineering* 130 (2), 021013.
- Bain, A.C., Meaney, D.F., 2000. Tissue-level thresholds for axonal damage in an experimental model of central nervous system white matter injury. *Journal of Biomechanical Engineering* 122, 615–622.
- Bayly, P.V., Black, E.E., Pedersen, R.C., 2006. In vivo imaging of rapid deformation and strain in an animal model of traumatic brain injury. *Journal of Biomechanics* 39, 1086–1095.
- Bilston, L.E., Liu, Z., Phan-Thien, N., 1997. Linear viscoelastic properties of bovine brain tissue in shear. *Biorheology* 34, 377–385.
- Bilston, L.E., Liu, Z., Phan-Tiem, N., 2001. Large strain behavior of brain tissue in shear: some experimental data and differential constitutive model. *Biorheology* 38, 335–345.
- Brands, D., Bovendeerd, P.H., Peters, G.W., Wismans, J.S., Paas, M., van Bree, J., 1999. Comparison of the dynamic behaviour of brain tissue and two model materials. In: Proceedings of the 43rd Stapp Car Crash Conference. pp. 313–333.
- Brands, D.W.A., Bovendeerd, P.H.M., Peters, G.W.M., 2000a. Finite shear behavior of brain tissue under impact loading. In: Proceedings of WAM2000, ASME Symposium on Crashworthiness, Occupant protection and Biomechanics in Transportation. 5–10 November, 2000, Orlando, Florida, USA.
- Brands, D.W.A., Bovendeerd, P.H.M., Peters, G.W.M., Wismans, J.S. H., 2000b. The large shear strain dynamic behavior of in-vitro porcine brain tissue and the silicone gel model material. In: Proceedings of the 44th Stapp Car Crash Conference. pp. 249–260.
- Brands, D.W.A., Peters, G.W.M., Bovendeerd, P.H.M., 2004. Design and numerical implementation of a 3-D non-linear viscoelastic constitutive model for brain tissue during impact. *Journal of Biomechanics* 37, 127–134.
- Brittany, C., Margulies, S.S., 2006. Material properties of porcine parietal cortex. *Journal of Biomechanics* 39, 2521–2525.
- Cheng, S., Bilston, L.E., 2007. Unconfined compression of white matter. *Journal of Biomechanics* 40, 117–124.
- Claessens, M., Sauren, F., Wismans, J., 1997. Modelling of the human head under impact conditions: a parametric study. In: Proceedings of the 41th Stapp Car Crash Conference. No. SAE 973338, pp. 315–328.
- Claessens, M.H.A., 1997. Finite Element Modelling of the Human Head Under Impact Conditions. Ph.D. dissertation. Eindhoven University of Technology, Eindhoven, The Netherlands.
- Darvish, K.K., Crandall, J.R., 2001. Nonlinear viscoelastic effects in oscillatory shear deformation of brain tissue. *Medical Engineering and Physics* 23, 633–645.
- Destrade, M., Gilchrist, M.D., Prikazchikov, D.A., Saccomandi, G., 2008. Surface instability of sheared soft tissues. *Journal of Biomechanical Engineering* 130, 0610071–0610076.
- Destrade, M., Murphy, J.G., Saccomandi, G., 2012. Simple shear is not so simple. *International Journal of Non-Linear Mechanics* 47, 210–214.
- Donnelly, B.R., Medige, J., 1997. Shear properties of human brain tissue. *Journal of Biomechanical Engineering* 119, 423–432.
- Elkin, B.S., Ilankovan, A.I., Morrison III, B., 2011. Dynamic, regional mechanical properties of the porcine brain: indentation in the coronal plane. *Journal of Biomechanical Engineering* 133, 071009.
- Estes, M.S., McElhaney, J.H., 1970. Response of Brain Tissue of Compressive Loading. ASME, Paper no. 70-BHF-13.
- Fallenstein, G.T., Hulce, V.D., Melvin, J.W., 1969. Dynamic mechanical properties of human brain tissue. *Journal of Biomechanics* 2, 217–226.
- Finan, J.D., Elkin, B.S., Pearson, E.M., Kalbian, I.L., Morrison III, B., 2012. Viscoelastic properties of the rat brain in the sagittal plane: effects of anatomical structure and age. *Annals of Biomedical Engineering* 40, 70–78.
- Franceschini, G., Bigoni, D., Regitnig, P., Holzapfel, G.A., 2006. Brain tissue deforms similarly to filled elastomers and follows

- consolidation theory. *Journal of the Mechanics and Physics of Solids* 54, 2592–2620.
- Fung, Y.C., 1967. Elasticity of soft tissues in simple elongation. *American Journal of Physiology* 213, 1532–1544.
- Fung, Y.C., 1993. *Biomechanics: Mechanical Properties of Living Tissues*, second ed. Springer-Verlag, New York.
- Fung, Y.C., Fronek, K., Patitucci, P., 1979. Pseudoelasticity of arteries and the choice of its mathematical expression. *American Journal of Physiology* 237, H620–H631.
- Funk, J.R., Hall, G.W., Crandall, J.R., Pilkey, W.D., 2000. Linear and quasi-linear viscoelastic characterization of ankle ligaments. *Journal of Biomechanical Engineering* 122, 15–22.
- Garo, A., Hrapko, M., van Dommelen, J.A.W., Peters, G.W.M., 2007. Towards a reliable characterization of the mechanical behaviour of brain tissue: the effects of postmortem time and sample preparation. *Biorheology* 44, 51–58.
- Gefen, A., Margulies, S.S., 2004. Are in vivo and in situ brain tissues mechanically similar?. *Journal of Biomechanics* 37, 1339–1352.
- Gennarelli, T.A., Thibault, L.E., Ommaya, A.K., 1972. Pathophysiologic responses to rotational and translational accelerations of the head. In: *Proceedings of the 16 Stapp Car Crash Conference*. SAE 720970, Detroit, MI, USA, pp. 296–308.
- Gent, A., 1996. A new constitutive relation for rubber. *Rubber Chemistry and Technology* 69, 59–61.
- Hirakawa, K., Hashizume, K., Hayashi, T., 1981. Viscoelastic properties of human brain—for the analysis of impact injury. *No To Shinkei* 33, 1057–1065.
- Ho, J., Kleiven, S., 2009. Can sulci protect the brain from traumatic injury. *Journal of Biomechanics* 42, 2074–2080.
- Holzappel, G.A., 2008. *Nonlinear Solid Mechanics. A Continuum Approach for Engineering*. John Wiley & Sons Ltd., Chichester, England.
- Horgan, C.O., 1995. Anti-plane shear deformations in linear and nonlinear solid mechanics. *SIAM Review* 37, 53–81.
- Horgan, C.O., Murphy, J.G., 2011. Simple shearing of soft biological tissues. *Proceedings of the Royal Society of London A* 467, 760–777.
- Horgan, C.O., Saccomandi, G., 2001. Anti-plane shear deformations for non-Gaussian isotropic, incompressible hyperelastic materials. *Proceedings of the Royal Society A: Mathematical, Physical and Engineering Sciences* 457 (2012), 1999–2017.
- Horgan, T.J., Gilchrist, M.D., 2003. The creation of three-dimensional finite element models for simulating head impact biomechanics. *International Journal of Crashworthiness* 8, 353–366.
- Hrapko, M., van Dommelen, J.A.W., Peters, G.W.M., Wismans, J.S.H.M., 2006. The mechanical behaviour of brain tissue: large strain response and constitutive modelling. *Biorheology* 43, 623–636.
- Hrapko, M., van Dommelen, J.A.W., Peters, G.W.M., Wismans, J.S.H.M., 2008. The influence of test conditions on characterization of the mechanical properties of brain tissue. *Journal of Biomechanical Engineering* 130, 0310031–03100310.
- Kleiven, S., 2007. Predictors for traumatic brain injuries evaluated through accident reconstructions. *Stapp Car Crash Journal* 51, 81–114.
- Kleiven, S., Hardy, W.N., 2002. Correlation of an FE model of the human head with local brain motion—consequences for injury prediction. *Stapp Car Crash Journal* 46, 123–144.
- Laksari, K., Shafeian, M., Darvish, K., 2012. Constitutive model for brain tissue under finite compression. *Journal of Biomechanics* 45, 642–646.
- LaPlaca, M.C., Cullen, D.K., McLoughlin, J.J., Cargill II, R.S., 2005. High rate shear strain of three-dimensional neural cell cultures: a new in vitro traumatic brain injury model. *Journal of Biomechanics* 38, 1093–1105.
- Lin, D.C., Shreiber, D.I., Dimitriadis, E.K., Horkay, F., 2008. Spherical indentation of soft matter beyond the Hertzian regime: numerical and experimental validation of hyperelastic models. *Biomechanics and Modeling in Mechanobiology* 8, 345–358.
- Lippert, S.A., Rang, E.M., Grimm, M.J., 2004. The high frequency properties of brain tissue. *Biorheology* 41, 681–691.
- Margulies, S.S., Thibault, L.E., 1989. An analytical model of traumatic diffuse brain injury. *Journal of Biomechanical Engineering* 111, 241–249.
- Margulies, S.S., Thibault, L.E., Gennarelli, T.A., 1990. Physical model simulations of brain injury in the primate. *Journal of Biomechanics* 23, 823–836.
- Meaney, D.F., Thibault, L.E., 1990. Physical model studies of cortical brain deformation in response to high strain rate inertial loading. In: *Proceedings of International Conference on the Biomechanics of Impacts*. IRCOBI, Lyon, France.
- Merodio, J., Ogden, R.W., 2005. Mechanical response of fiber-reinforced incompressible non-linearly elastic solids. *International Journal of Non-Linear Mechanics* 40, 213–227.
- Miller, K., Chinzei, K., 1997. Constitutive modelling of brain tissue: experiment and theory. *Journal of Biomechanics* 30, 1115–1121.
- Miller, K., Chinzei, K., 2002. Mechanical properties of brain tissue in tension. *Journal of Biomechanics* 35, 483–490.
- Mooney, M., 1964. Stress–strain curves of rubbers in simple shear. *Journal of Applied Physics* 35, 23–26.
- Morrison, B., Cater, H.L., Benham, C.D., Sundstrom, L.E., 2006. An in vitro model of traumatic brain injury utilizing two-dimensional stretch of organotypic hippocampal slice cultures. *Journal of Neuroscience Methods* 150, 192–201.
- Morrison III, B., Cater, H.L., Wang, C.C., Thomas, F.C., Hung, C.T., Ateshian, G.A., Sundstrom, L.E., 2003. A tissue level tolerance criterion for living brain developed with an in vitro model of traumatic mechanical loading. *Stapp Car Crash Journal* 47, 93–105.
- Morrison III, B., Meaney, D.F., Margulies, S.S., McIntosh, T.K., 2000. Dynamic mechanical stretch of organotypic brain slice cultures induces differential genomic expression: relationship to mechanical parameters. *Journal of Biomechanical Engineering* 122, 224–230.
- Nicolle, S., Lounis, M., Willinger, R., 2004. Shear properties of brain tissue over a frequency range relevant for automotive impact situations: new experimental results. *Stapp Car Crash Journal* 48, 239–258.
- Nicolle, S., Lounis, M., Willinger, R., Paliere, J.F., 2005. Shear linear behavior of brain tissue over a large frequency range. *Biorheology* 42, 209–223.
- Ogden, R.W., 1972. Large deformation isotropic elasticity—on the correlation of theory and experiment for incompressible rubber like solids. *Proceedings of the Royal Society of London: A—Mathematical and Physical Sciences* 326, 565–584.
- Ogden, R.W., 1997. *Non-Linear Elastic Deformations*. Dover New York.
- Ogden, R.W., Saccomandi, G., Sgura, I., 2004. Fitting hyperelastic models to experimental data. *Computational Mechanics* 34, 484–502.
- Ommaya, A.K., Hirsch, A.E., Martinez, J.L., 1966. The role of whiplash in cerebral concussion. In: *Proceedings of the 10th Car Crash Conference*. SAE 660804, Holloman Air Force Base, NM, USA, pp. 314–324.
- Pervin, F., Chen, W.W., 2009. Dynamic mechanical response of bovine grey matter and white matter brain tissues under compression. *Journal of Biomechanics* 42, 731–735.
- Pfister, B.J., Weihs, T.P., Betenbaugh, M., Bao, G., 2003. An in vitro uniaxial stretch model for axonal injury. *Annals of Biomedical Engineering* 31, 589–598.

- Prange, M.T., Margulies, S.S., 2002. Regional, directional, and age-dependent properties of the brain undergoing large deformation. *Journal of Biomechanical Engineering* 124, 244–252.
- Prange, M.T., Meaney, D.F., Margulies, S.S., 2000. Defining brain mechanical properties: effects of region, direction and species. In: *Proceedings of the 44th Stapp Car Crash Conference*. pp. 205–213.
- Rashid, B., Destrade, M., Gilchrist, M.D., 2012a. A high rate tension device for characterizing brain tissue. *Journal of Sports Engineering and Technology*: 226 (3/4), 170–176.
- Rashid, B., Destrade, M., Gilchrist, M.D., 2012b. Mechanical characterization of brain tissue in compression at dynamic strain rates. *Journal of the Mechanical Behavior of Biomedical Materials* 10, 23–38.
- Ruan, J., Khalil, T., King, A., 1994. Dynamic response of the human head to impact by three—dimensional finite element analysis. *Journal of Biomechanical Engineering* 116, 44–50.
- Shen, F., Tay, T.E., Li, J.Z., Nigen, S., Lee, P.V.S., Chan, H.K., 2006. Modified Bilston nonlinear viscoelastic model for finite element head injury studies. *Journal of Biomechanical Engineering* 128, 797–801.
- Shuck, L.Z., Advani, S.H., 1972. Rheological response of human brain tissue in shear. *ASME Journal of Basic Engineering* 94, 905–911.
- Takhounts, E.G., Crandall, J.R., Darvish, K.K., 2003a. On the importance of nonlinearity of brain tissue under large deformations. *Stapp Car Crash Journal* 47, 107–134.
- Takhounts, E.G., Eppinger, R.H., Campbell, J.Q., Tannous, R.E., Power, E.D., Shook, L.S., 2003b. On the development of the SIMOn finite element head model. *Stapp Car Crash Journal* 47, 107–133.
- Tamura, A., Hayashi, S., Nagayama, K., Matsumoto, T., 2008. Mechanical characterization of brain tissue in high-rate extension. *Journal of Biomechanical Science and Engineering* 3, 263–274.
- Tamura, A., Hayashi, S., Watanabe, I., Nagayama, K., Matsumoto, T., 2007. Mechanical characterization of brain tissue in high-rate compression. *Journal of Biomechanical Science and Engineering* 2, 115–126.
- Thibault, K.L., Margulies, S.S., 1998. Age-dependent material properties of the porcine cerebrum: effect on pediatric inertial head injury criteria. *Journal of Biomechanics* 31, 1119–1126.
- Trexler, M.M., Lennon, A.M., Wickwire, A.C., Harrigan, T.P., Luong, Q.T., Graham, J.L., Maisano, A.J., Roberts, J.C., Merkle, A.C., 2011. Verification and implementation of a modified split Hopkinson pressure bar technique for characterizing biological tissue and soft biosimulant materials under dynamic shear loading. *Journal of the Mechanical Behavior of Biomedical Materials* 4, 1920–1928.
- Velardi, F., Fraternali, F., Angelillo, M., 2006. Anisotropic constitutive equations and experimental tensile behavior of brain tissue. *Biomechanics and Modeling in Mechanobiology* 5, 53–61.
- Zhang, L., Yang, K.H., Dwarampudi, R., Omori, K., Li, T., Chang, K., Hardy, W.N., Khalil, T.B., King, A.I., 2001. Recent advances in brain injury research: a new human head model development and validation. *Stapp Car Crash Journal* 45, 369–393.